Available online at www.sciencedirect.com
ScienceDirect
Icarus 189 (2007) 196–212
ICARUS
www.elsevier.com/locate/icarus

Models of the collisional damping scenario for ice-giant planets and Kuiper belt formation

Harold F. Levison [a,*], Alessandro Morbidelli [b]

[a] *Department of Space Studies, Southwest Research Institute, Boulder, CO 80302, USA*
[b] *Observatoire de la Côte d'Azur, Nice, France*

Received 2 June 2006; revised 8 January 2007

Available online 1 February 2007

Abstract

Chiang et al. [Chiang, E., Lithwick, Y., Murray-Clay, R., Buie, M., Grundy, W., Holman, M., 2007. In: Protostars and Planets V, pp. 895–911] have recently proposed that the observed structure of the Kuiper belt could be the result of a dynamical instability of a system of ∼5 primordial ice-giant planets in the outer Solar System. According to this scenario, before the instability occurred, these giants were growing in a highly collisionally damped environment according to the arguments in Goldreich et al. [Goldreich, P., Lithwick, Y., Sari, R., 2004. Astrophys. J. 614, 497–507; Annu. Rev. Astron. Astrophys. 42, 549–601]. Here we test this hypothesis with a series of numerical simulations using a new code designed to incorporate the dynamical effects of collisions. We find that we cannot reproduce the observed Solar System. In particular, Goldreich et al. [Goldreich, P., Lithwick, Y., Sari, R., 2004. Astrophys. J. 614, 497–507; Annu. Rev. Astron. Astrophys. 42, 549–601] and Chiang et al. [Chiang, E., Lithwick, Y., Murray-Clay, R., Buie, M., Grundy, W., Holman, M., 2007. In: Protostars and Planets V, pp. 895–911] argue that during the instability, all but two of the ice giants would be ejected from the Solar System by Jupiter and Saturn, leaving Uranus and Neptune behind. We find that ejections are actually rare and that instead the systems spread outward. This always leads to a configuration with too many planets that are too far from the Sun. Thus, we conclude that both Goldreich et al.'s scheme for the formation of Uranus and Neptune and Chiang et al.'s Kuiper belt formation scenario are not viable in their current forms.

Keywords: Planetary formation; Kuiper belt; Origin, Solar System; Planetary dynamics

1. Introduction

The investigation of the primordial processes that sculpted the structure of the Kuiper belt is still an active topic of research. Several models have been developed over the last decade, based on the effects of Neptune's migration on the distant planetesimal disk (Malhotra, 1995; Hahn and Malhotra, 1999; Gomes, 2003; Levison and Morbidelli, 2003; see Morbidelli et al., 2003 for a review). However, many aspects of the Kuiper belt have not yet been fully explained. Moreover, a new paradigm about the giant planets orbital evolution has recently been proposed (Tsiganis et al., 2005; Gomes et al., 2005; see Morbidelli, 2005 or Levison et al., 2006 for reviews), which calls for a global revisiting of the Kuiper belt sculpting problem.

In this evolving situation, Chiang et al. (2007) have recently proposed an novel scenario. The idea is based on a recent pair of papers by Goldreich et al. (2004a, 2004b), who, based on analytic arguments, predicted that originally roughly five planets began to grow between ∼20 and ∼40 AU. However, as these planets grew to masses of ∼15 $M_\oplus$ their orbits went unstable, all but two of them were ejected, leaving Uranus and Neptune in their current orbits. Chiang et al. (2007) argued that this violent process could explain the structure of the Kuiper belt that we see today. We review the Chiang et al.'s (2007) scenario in more detail in Section 2. Like Goldreich et al. (2004a, 2004b), the Chiang et al.'s (2007) scenario was not tested with numerical simulations, but was solely supported by order-of-magnitude analytic estimates, which were only possible under a number of simplifications and assumptions.

Therefore, the goal of this paper is to simulate numerically Chiang et al.'s (2007) scenario, in order to see if the presence

* Corresponding author.
E-mail address: hal@boulder.swri.edu (H.F. Levison).

0019-1035/$ – see front matter
doi:10.1016/j.icarus.2007.01.004

of five Neptune mass bodies (or a similar configuration) in a primordial planetesimal disk is indeed consistent with the observed structure of the outer Solar System (the orbital distribution of the Kuiper belt and of the planets). Because Goldreich et al.'s (2004a, 2004b) and Chiang et al.'s (2007) scenarios heavily rely on the presence of a highly collisional planetesimal disk, we need first to develop a new numerical integrator that takes collisions into account as well as their effects on the dynamical evolution. This code is described and tested in Section 3. In Section 4 we then describe the results of the simulations that we did of Chiang et al.'s (2007) scenario. The conclusions and the implications are discussed in Section 5.

2. A brief description of the Goldreich et al.'s (2004a, 2004b)/Chiang et al.'s (2007) scenario

As we discussed above, Chiang et al.'s (2007) scenario for sculpting the Kuiper belt is built on Goldreich et al.'s (2004a, 2004b) scheme for planet formation. In Goldreich et al. (2004a, 2004b), the authors pushed to an extreme the concept of runaway (Ohtsuki and Ida, 1990; Kokubo and Ida, 1996) and oligarchic growth (Kokubo and Ida, 1998; Thommes et al., 2003; Chambers, 2006) of protoplanets in planetesimal disks. Unlike previous works, they assumed that the bulk of the mass of the planetesimal disk is in particles so small (submeter to cm in size) that they have very short mean free paths. In this situation the disk is highly collisional, and the collisional damping is so efficient that the orbital excitation passed from the growing planets to the disk is instantaneously dissipated. With this set-up, the extremely cold disk exerts a very effective and time enduring dynamical friction on the growing planetary embryos, whose orbital eccentricities and inclinations remain very small. Consequently, the embryos grow quickly, accreting the neighboring material due to the fact that gravitational focusing is large.

The order-of-magnitude analytic estimates that describe this evolution lead to the conclusion that the system reaches a steady state consisting of a chain of planets, separated by 5 Hill radii embedded in a sea of small particles. As the planets grow, their masses increase while their number decreases. This process continues until the surface density of the planetary embryos, Σ, is roughly equal to that of the disk, σ. If the mass of the disk is tuned to obtain planets of Uranus/Neptune mass when $\Sigma \sim \sigma$ then the conclusion is that about 5 of these planets had to form in the range 20–40 AU.

Goldreich et al. (2004a, 2004b) argue that when $\Sigma \sim \sigma$ the dynamical friction exerted on the planets by the disk is no longer sufficient to stabilize the planetary orbits. Consequently, the planets start to scatter one another onto highly elliptical and inclined orbits. They assume that all but two of the original ice planets (i.e., three of five in the nominal case) are ejected from the Solar System in this scattering process (no attempts were made to model this event). Once their companions have disappeared, the two remaining planets feel a much weaker excitation, and therefore their orbits can be damped by the dynamical friction exerted by the remaining disk. This damping phase is then followed by a period of outward migration (Fernández and Ip, 1984). They therefore become Uranus and Neptune, with quasi-circular co-planar orbits at ∼20 and ∼30 AU.

Chiang et al. (2007) argue that this basic scenario, with some small modifications, can explain much of the structure currently seen in the Kuiper belt. The Kuiper belt displays a very complex dynamical structure. For our purposes, four characteristics of the Kuiper belt are important: (1) The Kuiper belt apparently ends near 50 AU (Trujillo and Brown, 2001; Allen et al., 2001, 2002). (2) The Kuiper belt appears to consist of at least two distinct populations with different dynamical and physical properties (Brown, 2001; Levison and Stern, 2001; Trujillo and Brown, 2002; Tegler and Romanishin, 2003). One group is dynamically quiescent and thus we call it the *cold population*. All the objects in this population are red in color. The other group is dynamically excited, inclinations can be as large as 40°, and thus we call it the *hot population*. It, too, contains red objects, but it also contains about as many objects that are gray in color. The largest objects in the Kuiper belt reside in the hot population. (3) Many members of the hot population are trapped in the mean motion resonances (MMRs) with Neptune. The most important of these is the 2:3 MMR, which is occupied by Pluto. (4) The Kuiper belt only contains less than roughly 0.1 $M_\oplus$ of material (Jewitt et al., 1996; Chiang and Brown, 1999; Trujillo et al., 2001; Gladman et al., 2001; Bernstein et al., 2004). This is surprising given that accretion models predict that $\gtrsim$10 $M_\oplus$ must have existed in this region in order for the objects that we see to grow (Stern, 1996; Stern and Colwell, 1997; Kenyon and Luu, 1998, 1999).

Chiang et al. (2007) suggest the following explanation for the Kuiper belt's structure. First, in order to make the edge (characteristic 1 above), they assume that the planetesimal disk is truncated at ∼47 AU. This assumption is legitimate given the work of Youdin and Shu (2002) and Youdin and Chiang (2004) on planetesimal formation. They assume—as a variant of the pure Goldreich et al.'s (2004a, 2004b) scenario—that some coagulation actually occurred in the planetesimal disk while the planets were growing. This coagulation produced a population of objects with a size distribution and a total number comparable to the hot population that we see today. Because this population constitutes only a small fraction of the total disk's mass, their existence does not change the overall collisional properties of the disk, which are essential for Goldreich et al.'s (2004a, 2004b) story.

Thus, during the final growth of the ice giants, Chiang et al. (2007) envision three distinct populations: the 'planetary embryos' (objects that eventually become Neptune-sized), the 'KBOs' (macroscopic objects of comparable size to the current Kuiper belt objects, formed by coagulation), and 'disk particles' (golf-ball sized planetesimals that constitute the bulk of the disk's mass and which have a very intense collision rate and damping). The KBOs are not massive enough to be affected by dynamical friction, but are big enough not to be damped by collisions with the disk-particles.

As the planets grow to their final sizes, Chiang et al. (2007) estimate that the KBOs can be scattered by the growing planets to orbits with eccentricities and inclinations of order of 0.2. These, they argue, become the hot population, which has ob-

served eccentricities and inclinations comparable to these values. After all but two of the original planets are removed by the dynamical instability and the ice giants evolve onto their current orbits inside of 30 AU, Chiang et al. (2007) suggest that there is still a population of very small disk particles between 40 and 47 AU. With the planets gone, this disk can become dynamically cold enough to allow large objects to grow in it, producing a second generation of KBOs on low-eccentricity and low-inclination orbits. These objects should be identified, in Chiang et al.'s (2007) scenario, with the observed cold population of the Kuiper belt.

The mass of the disk between 40 and 47 AU, however, should retain on order of half of its original mass, namely about 20 $M_\oplus$ according to the surface density assumed in Chiang et al.'s (2007) Eq. (13). How this total mass was lost and how the cold population acquired its current, non-negligible eccentricity excitation, are not really explained by Chiang et al. (2007). The authors limit themselves to a discussion of the radial migration of Neptune, after the circularization of its orbit, to create the resonant populations (Malhotra, 1995; Hahn and Malhotra, 1999). This, in principal, might excite the cold classical belt, although Chiang et al. (2007) admit that it is not at all obvious how planet migration would proceed in a highly collisional disk. As for the mass depletion, collisional grinding is the only mechanism that makes sense at this point in time. However, it is not clear (at least to us) why collisional grinding would become so effective at this late stage while it was negligible during the planet formation and removal phases, when the relative velocities were much higher.

At this point we want to emphasize that, although the ideas presented in Goldreich et al. (2004a, 2004b) and Chiang et al. (2007) are new and intriguing, the papers do not present any actual models. Most of the arguments are based on order-of-magnitude equations where factors of 2 and $\sqrt{3}$ are dropped and approximate timescales are set equal to one another in order to determine zeroth-order steady state solutions. In addition, simplifications are made to make the problem tractable analytically, like, for example, at any given instant all of the disk particles have the same size. Another example of a simplification is that the rate of change of the velocity dispersion of the disk particles due to collisions is simply set to the particle-in-the-box collision rate—the physics of the collisions are ignored. While making such approximations is reasonable when first exploring an idea and determining whether it could possibly work, numerical experiments are really required in order to determine whether the process does indeed act as the analytic expressions predict.

Finally, many of the steps in these scenarios are not justified. Of particular interest to us is the stage when, according to Goldreich et al. (2004a, 2004b), all but two (i.e., three of five in the nominal case) of the original ice giants are removed from the system via a gravitational instability. The papers present order-of-magnitude equations that argue that such an instability would occur, but the authors are forced to speculate about the outcome of this event.

Indeed, we suspect, based on our experiences, that Goldreich et al.'s (2004a, 2004b) expectations about the removal of the ice giants are naive. In particular, Levison et al. (1998) followed the dynamical evolution of a series of fictitious giant planet systems during a global instability. They found that during the phase when planets are scattering off of one another, the planetary system spreads to large heliocentric distances, and, while planets can be removed by encounters, the outermost planet is the most likely to survive. Similarly, Morbidelli et al. (2002) studied systems of planetary embryos of various masses originally in the Kuiper belt and found that in all cases the embryos spread and some survived at large heliocentric distances. From these works we might expect that Goldreich et al.'s (2004a, 2004b) instability would lead to an ice giant at large heliocentric distances (but still within the observation limits), rather than having a planetary system that ends at 30 AU with a disk of small particles beyond. Granted, the simulations in both Levison et al. (1998) and Morbidelli et al. (2002) did not include a disk of highly damped particles that can significantly affect the evolution of the planets, so new simulations are needed to confirm or dismiss the Goldreich et al.'s (2004a, 2004b)/Chiang et al.'s (2007) scenario. In this paper we perform such simulations. We are required to develop a new numerical integration scheme to account for the collisional damping of the particle disk. This scheme is detailed and tested in the next section.

3. The code

In this section we describe, in detail, the code that we constructed to test the Chiang et al. (2007) scenario. Before we can proceed, however, we must first discuss what physics we need to include in the models. As we described above, our motivation is to determine how a system containing a number of ice-giant planets embedded in a disk of collisionally damped particles dynamically evolves with time. Our plan is to reproduce the systems envisioned by Goldreich et al. (2004a, 2004b) and Chiang et al. (2007) as closely as possible rather than create the most realistic models that we can. Thus, we purposely adopt some of the same assumptions employed by Goldreich et al. (2004a, 2004b). For example, although Goldreich et al. (2004a, 2004b) invoke a collisional cascade to set up the systems that they study, their formalism assumes that the disk particles all have the same size and ignore the effects of fragmentation and coagulation. We make the same assumption.

In addition, although Goldreich et al. (2004a, 2004b) invoke a collisional cascade to grind kilometer-sized planetesimals to submeter-sized disk particles, they implicitly assume that the timescale to change particle size is short compared to any of the dynamical timescales in the problem. Thus, their analytic representation assumes that the radius of the disk particles, s, is fixed. They determine which s to use by arguing that disk particles will grind themselves down until the timescale for the embryos to excite their orbits is equal to the collisional damping time (which is a function of s). Then s is held constant. We, therefore, hold s constant as well. Also, Goldreich et al. (2004a, 2004b) do not include the effects of gas drag in their main derivations, we again follow their lead in this regard.

Our code is based on SyMBA (Duncan et al., 1998; Levison and Duncan, 2000). SyMBA is a symplectic algorithm that has

the desirable properties of the sophisticated and highly efficient numerical algorithm known as Wisdom–Holman Map (WHM), (Wisdom and Holman, 1991) and that, in addition, can handle close encounters (Duncan et al., 1998). This technique is based on a variant of the standard WHM, but it handles close encounters by employing a multiple time step technique introduced by Skeel and Biesiadecki (1994). When bodies are well separated, the algorithm has the speed of the WHM method, and whenever two bodies suffer a mutual encounter, the time step for the relevant bodies is recursively subdivided.

Although SyMBA represented a significant advancement to the state-of-art of integrating orbits, it suffers from a basic and serious limitation. At each time step of the integration, it is necessary to calculate the mutual gravitational forces between all bodies in the simulation. If there are N bodies, one therefore requires N^2 force calculations per time step, because every object needs to react to the gravitational force of every other body. Thus, even with fast clusters of workstations, we are computationally limited to integrating systems where the total number of bodies of the order of a few thousand.

Yet, in order to follow both the dynamical and collisional evolution of the numerous small bodies present during the Goldreich et al.'s (2004a, 2004b) scenario, we need to implement a way to follow the behavior of roughly 10^{26-29} particles. This clearly is beyond the capabilities of direct orbit integrators. Only statistical methods can handle this number of objects. In the following, we describe our approach to this problem.

As described above, the systems that Chiang et al.'s (2007) envisions have three classes of particles: the planetary embryos, the KBOs, and the disk particles. Each class has its unique dynamical characteristics. The embryos are few in number and their dynamics are not directly effected by collisional damping. Thus, in our new code, which we call *SyMBA_COL*, they can be followed directly in the standard N-body part of SyMBA. The KBOs are not dynamically important to the system from either a dynamical or collisional point of view. Since we are more concerned here with the final location of the ice giants than the dynamical state of the Kuiper belt, we ignore this population. Finally, we need to include a very large population of submeter-sized particles that both dynamically interact with the rest of the system and collisionally interact with each other.

Thus, we have added a new class of particle to SyMBA which we call a *tracer* particle. Each tracer is intended to represent a large number of disk particles on roughly the same orbit as one another. Each tracer is characterized by three numbers: the physical radius s, the bulk density ρ_b, and the total mass of the disk particles represented by the tracer, $m_{\rm tr}$. For example, the runs presented below, we set $s = 1$ cm or 1 m and $\rho_b = 1\ {\rm g\,cm^{-3}}$. In addition, we typically want to represent a $\sim$75 $M_\oplus$ disk with $\sim$3000 tracer particles, meaning that $m_{\rm tr} \sim 0.025\ M_\oplus$ (although the exact numbers vary from run to run).

The first issue we needed to address when constructing SyMBA_COL, was to determine an algorithm that correctly handles the gravitational interaction between the embryos and the disk particles. Since there are only a few embryos and they are relatively large, the acceleration of the tracers due to the embryos can be determined using the normal N-body part of SyMBA. It is less obvious, however, whether the gravitational effect of the disk particles on the embryos can also be effectively simulated using the normal N-body part of SyMBA, i.e., using the forces directly exerted on the embryos by the tracers. To argue this position, let us point out that the gravitational effect of the disk particles on the embryos is well approximated by the *dynamical friction* formalism, which, assuming a Maxwellian velocity distribution, can be written as (Chandrasekhar, 1943; also see Binney and Tremaine, 1987):

$$\frac{{\rm d}\vec{w}}{{\rm d}t} \propto \frac{(m_{\rm em} + m_{\rm dp})\rho_{\rm disk}}{w^3}\left[{\rm erf}(X) - \frac{2X}{\sqrt{\pi}}e^{-X^2}\right]\vec{w}, \tag{1}$$

where $X \equiv w/(\sqrt{2}u)$, w is the velocity of the embryo, u is the velocity dispersion of the disk particles, $m_{\rm dp}$ is that mass of an individual disk particle, 'erf' is the error function, and $\rho_{\rm disk}$ is the background volume density of the disk. So, if $m_{\rm em} \gg m_{\rm dp}$, the acceleration of the embryos due to the disk is independent on the mass of individual disk particles. Thus, although $m_{\rm tr} \gg m_{\rm dp}$, the direct acceleration of the embryos due to the tracers is roughly the same as if we had each individual disk particle in the simulation as long as $m_{\rm tr} \ll m_{\rm em}$. Therefore, in general, we can employ the standard N-body part of the SyMBA to calculate the gravitational effects of the embryos and the disk particles on each other. We return to the issue of how big $m_{\rm em}/m_{\rm tr}$ needs to be below.

All that is left is to consider the effects of the disk particles on each other. There are two effects that must be included: collisional damping and self-gravity. We handle the former through Monte Carlo techniques. The first step in our collisional algorithm is to divide the Solar System into a series of logarithmically spaced annular rings that, in the simulations performed here, stretched from 10 to 60 AU. As we describe more below, the logarithmic spacing is employed by the self-gravity algorithm. In all, we divided space into $N_{\rm ring} = 1000$ such rings in our production runs (although in some of our tests, we used $N_{\rm ring} = 10{,}000$ rings). We use these rings to statistically keep track of the state of the disk particles. In particular, as the simulation progresses, we keep track of the tracer particles moving through the ring and from this calculate: (1) the total mass of disk particles in that ring (M_a), and (2) the vertical velocity dispersion of the disk particles, u_z. These values are recalculated every $\tau_{\rm update}$, by moving each tracer along its Kepler orbit in the barycentric frame and adding its contribution to each ring as it passes through. Except where noted, we set $\tau_{\rm update} = 200$ yr. In addition, as the tracers orbit during the simulation, we keep a running list of their velocities and longitudes as they pass through each individual ring. Entries are dropped from this list if they are older than $\tau_{\rm update}$.

At each timestep in the simulation, we evaluate the probability, p, that each tracer particle will suffer a collision with another disk particle based on the particle-in-a-box approximation. In particular, $p \equiv n(4\pi s^2)w\,{\rm d}t$, where n is the local number density of the disk particles, w is the velocity of the tracer relative to the mean velocity of the disk, and ${\rm d}t$ is the timestep. It is important to note that n is not the number density of tracers, but the number density of the disk assuming that all

disk particles had a radius of s. Therefore, p does not carry any information about the mass or number of tracers, but is only dependent on the surface density of the disk, its vertical velocity dispersion, and s. In addition, the analytic derivations in Goldreich et al. (2004a, 2004b) usually assume that $w = u$, however, here we use the true velocity of the individual tracer.

We assume that

$$n(z) = \begin{cases} (1 - \exp[-1])n_0, & \text{if } z < z_0, \\ n_0 \exp[-z/z_0], & \text{if } z \geqslant z_0, \end{cases} \tag{2}$$

where z is the distance above the disk mid-plane, $n_0 = M_a/2(\frac{4}{3}\pi s^3 \rho_b) z_0 A_a$, A_a is the area of the ring, and z_0 is the scale height of the disk. In particular, $z_0 = u_z/\Omega$, where Ω is the orbital frequency. We hold $n(z)$ constant for $z < z_0$ to help correct for the fact that dt is finite. If we did not hold n constant there would be a danger that we would underestimate the collision rates because particles would jump over the high density mid-plane as they orbit. The price to pay for this is a discontinuity in $n(z)$ at z_0, but it is a price, we believe, that is wise to pay.

Once we have determined p, we generate a random number between 0 and 1, and if p is larger than this number, we declare that the tracer has suffered a collision with another disk particle. Now, we need to determine the velocity of the impactor, and again we turn to our rings. As we stated above, as the tracers orbit during the simulation, we keep a running list of particles that had passed through each ring, keeping tract of their individual velocities. The impactor is assumed to have the same location as the target, but its velocity is chosen from this running list appropriately rotated assuming cylindrical symmetry. We also assume that two particles bounce off of one another [as in Goldreich et al. (2004a, 2004b)], but that the coefficient of restitution is very small. The end result is that we change the velocity of our target tracer to be the mean of its original velocity and that of the impactor.

We have to spend a little time discussing how we decide which velocity in our running list to choose because if this is done incorrectly it leads to a subtle error in the results. In an early version of the code we simply chose the velocity at random. This is the same as assuming that the disk is axisymmetric, and thus collisions try to force particles onto circular orbits. However, in a situation where the disk is interacting with a massive planet on an eccentric orbit, the natural state of the disk is for its particles to evolve onto eccentric orbits whose longitude of perihelion, $\tilde{\omega}$, is the same as the planet's, and whose eccentricity, e, is a function of the eccentricity of the planet and the distance from the planet. In essence, this situation should produce an eccentric ring. Experimenting with our original code showed that in situations where the ring is massive, the assumption of axisymmetry causes the planet to migrate away from the disk at an unphysically large rate, as collisions try to force particles onto circular orbits while the planet tries to excite their eccentricities.

Thus, we found that our code needs to be able to support eccentric rings. We found that we can accomplish this by modifying the method we use for choosing a velocity for the impactor. In particular, in addition to storing a particle's velocity in the running list, we also keep tract of its true longitude, λ. We choose from the running list the velocity of the object that has the λ closest to that of the target tracer. In this way, asymmetries can be supported by the code. We show an example of this in the test section below.

Through experimentation we also found that we need to include self-gravity between the disk particles, at least crudely. In an early version of the code we did not include this effect and found that under certain conditions there was an unphysical migration of planetary embryos. In particular, in situations where disk particles became trapped in a MMR with an embryo (particularly the 1:1 MMR) the embryo was incorrectly pushed around by the disk particles if there was a large number of additional disk particles in the system. This did not occur if the particle self-gravity was included.

There are too many tracers in our simulations to include self-gravity directly. Thus, we employ a technique originally developed for the study of disk galaxies, known as the particle-mesh (PM) method (Miller, 1978). In what follows, we use the formalism from Binney and Tremaine (1987). We first define a modified polar coordinate system $u \equiv \ln \varrho$ and ϕ, where ϱ and ϕ are the normal polar coordinates, and define a *reduced* potential, $V(\mathrm{u}, \phi) = e^{u/2}\Phi[\varrho(\mathrm{u}), \phi]$ and a *reduced* surface density $S(\mathrm{u}, \phi) = e^{\mathrm{u}/2}\sigma[\varrho(\mathrm{u}), \phi]$ such that

$$V(\mathrm{u}, \phi) = -\frac{G}{\sqrt{2}} \int_{-\infty}^{\infty} \int_{0}^{2\pi} \frac{S(\mathrm{u}', \phi')\, \mathrm{d}\phi'}{\sqrt{\cos(\mathrm{u} - \mathrm{u}') - \cos(\phi - \phi')}}\, \mathrm{du}'. \tag{3}$$

If we break the disk into cells this becomes

$$V_{lm} \approx \sum_{l'} \sum_{m'} \mathcal{G}(l' - l, m' - m) \mathcal{M}_{l'm'}, \tag{4}$$

where $\mathcal{M}_{lm} = \iint_{\mathrm{cell}(l,m)} S\, \mathrm{du}\, \mathrm{d}\phi$ and $\mathcal{G}$ is the Green's function:

$$\mathcal{G}(l' - l, m' - m) = -\frac{G}{\sqrt{2(\cosh(\mathrm{u}_{l'} - \mathrm{u}_l) - \cos(\phi_{m'} - \phi_m))}}, \tag{5}$$

when $l \neq l'$ and $m \neq m'$, and

$$\mathcal{G}(0, 0) = -2G\left[\frac{1}{\Delta\phi} \sinh^{-1}\left(\frac{\Delta\phi}{\Delta \mathrm{u}}\right) + \frac{1}{\Delta \mathrm{u}} \sinh^{-1}\left(\frac{\Delta \mathrm{u}}{\Delta\phi}\right)\right], \tag{6}$$

where Δu and $\Delta\phi$ are the grid spacings.

For this algorithm we found that it is best to assume that the disk is axisymmetric, so Eq. (4) becomes

$$\begin{aligned} V_{lm} &\approx \sum_{l'} \sum_{m'} \mathcal{G}(l' - l, m' - m) \frac{\Delta\phi}{2\pi} \mathcal{M}_{l'} \\ &= \sum_{l'} \frac{\Delta\phi}{2\pi} \mathcal{M}_{l'} \sum_{m'} \mathcal{G}(l' - l, m' - m), \end{aligned} \tag{7}$$

$$V_l \approx \sum_{l'} \frac{\Delta\phi}{2\pi} \mathcal{M}_{l'} \tilde{\mathcal{G}}(l' - l). \tag{8}$$

Note that Eq. (8) is one-dimensional, and thus it only supplies us with a radial force. The tangential and vertical forces are assumed to be zero. We made this assumption due to the small

number of tracers in our system. However, a simple radial force is adequate for our purposes.

Also, the form of Eq. (8) allows us to use the rings already constructed for the collisional algorithm. All we need is that relationship between $\mathcal{M}_{l'}$ and the total amount of mass in ring, M_a. We find that

$$\mathcal{M}_{l'} = \frac{2M_a}{(a_{l2}^2 - a_{l1}^2)} a_l^{3/2} \left[\ln(a_{l2}) - \ln(a_{l1})\right], \tag{9}$$

where a_{l2}, a_{l1}, and a_l are the outer edge, inner edge, and radial center of ring l.

So, Eq. (8) gives us the reduced potential at the center of ring l and thus the true potential can be found ($\Phi = e^{-u/2} V$). To calculate the radial acceleration at any location, we employ a cubic spline interpolation scheme. Finally, the acceleration of a particle is calculated by numerically differentiating this interpolation.

3.1. Tests

In this subsection we describe some of the tests that we performed on SyMBA_COL.

3.1.1. An isolated ring

In this test, we studied the behavior of a disk of particles initially on eccentric orbits as collisions damp their relative velocities. In particular, we evolved a system containing the Sun and 1000 tracers, which were uniformly spread in semi-major axis from 30 to 35 AU. Initially, the tracers were given a Raleigh distribution with an RMS eccentricity equal to 0.1, and an RMS $\sin(i)$ equal to 0.05. The total mass of the ring was 10 $M_\oplus$ and we set $s = 1$ cm.

The solid curve in Fig. 1 shows the temporal evolution of the eccentricities in the above system. As the system evolved, the ring collapsed (i.e., eccentricities and inclinations dropped) as the collisions damped out random velocities. During this process, we found that a small fraction of the particles were left behind because as the ring collapsed these particles found themselves in regions of space where there were no other particles. For example, if a particle had a relatively large initial inclination and happened not to have suffered a collision early on, then it can be left behind on a large inclination orbit because it finds itself traveling above and below the collapsing disk most of the time. Eventually, it will hit another particle because it penetrates the disk, but this can take a long time. The end result of this process is that during the collapse, there is always a high velocity tail to the eccentricity and inclination distributions. To correct for this, we plot the median eccentricity rather than the more standard RMS eccentricity in Fig. 1. In this system, we find that the e-folding damping time of the eccentricity is 320 years.

In order to test whether our code has converged we performed a second experiment. Recall that in the first run, we used 1000 tracers, $N_{\rm ring} = 1000$, and $\tau_{\rm update} = 200$ yr. This produced the solid curve in the figure. The dotted curve shows the results for a high resolution run where $N_{\rm ring} = 10{,}000$, $\tau_{\rm update} = 20$ yr, and we used 10,000 tracer particles. Although there are some

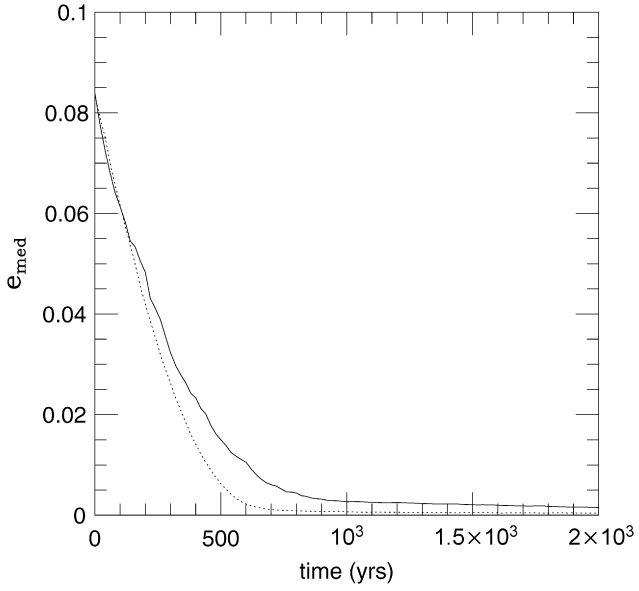

Fig. 1. The temporal evolution of the collisionally active ring of particles used as the first test of our new code. In particular, we plot the median eccentricity ($e_{\rm med}$). The solid and dotted curves refer to the normal and HIRES runs, respectively.

differences between the two curves, the basic evolution of the systems, including their e-folding damping times, are the same. Thus, we feel that the code has converged well enough that we can employ the lower resolution.

We now need to calculate what Goldreich et al.'s (2004a, 2004b) development would predict. Goldreich et al.'s (2004a, 2004b) Eq. (50) states that

$$\frac{1}{\tau_{\rm col}} \equiv -\frac{1}{u}\frac{{\rm d}u}{{\rm d}t} \sim \Omega \frac{\sigma}{\rho_b s}. \tag{10}$$

Plugging in the appropriate values for this test, we find that Goldreich et al. (2004a, 2004b) predict that the collisional damping time, $\tau_{\rm col}$, should be ~110 yr, which is about a factor of 3 shorter than we observed. However, we believe that the agreement is reasonably good because Goldreich et al.'s (2004a, 2004b) derivations were intended to be order-of-magnitude in nature and that factors of a few were typically dropped.

3.1.2. A narrow ring with a giant planet

As discussed above, we found that our code must be able to support an eccentric ring if the dynamics demand it, and we described our methods for doing so. Here we present a test of this ability. In particular, we studied the behavior of a 10 $M_\oplus$ narrow ring of collisional particles under the gravitational influence of Saturn. In order to enhance the eccentricity forcing of the ring, we set Saturn's $e = 0.2$. The semi-major axes (a) of the disk particles was spread from $1.70 < a/a_{\rm Sat} < 1.72$, where $a_{\rm Sat}$ is Saturn's semi-major axis. The particles had an initial eccentricity of 0.1. Of importance here, the initial $\tilde{\omega}$ was randomly chosen from the range of 0 and 2π. Thus, if we define two new variables, $H \equiv e\cos(\tilde{\omega})$ and $K \equiv e\sin(\tilde{\omega})$, then at $t = 0$ the tracer particles fall along a circle of radius e in H–K space (Fig. 2).

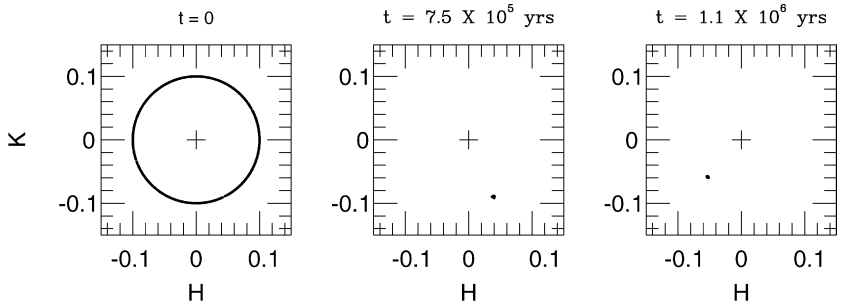

Fig. 2. Three snapshots of the evolution of a ring of collisionally active particles under the gravitational influence of a Saturn-mass planet with $e = 0.2$. The ring has a semi-major axis 1.71 times larger than the planet. The particles, which were initially uniform in $\tilde{\omega}$ ($H \equiv e\cos(\tilde{\omega})$ and $K \equiv e\sin(\tilde{\omega})$), clump in $\tilde{\omega}$ and thus form an eccentric ring.

We find that as the system settles down, the particles evolve to a point in H–K space (Fig. 2). And since this point does not sit at the origin, the particles have the same e and $\tilde{\omega}$, i.e., they form an eccentric ring. Unfortunately, we know of no analytic theory describing the behavior of this ring. However, we can take a clue from the secular theory of the response of a massless test particle to an eccentric planet (Brouwer and Clemence, 1961; see also Murray and Dermott, 2000), which predicts that the 'forced' eccentricity of the particle is

$$e_{\text{forced}} = \frac{b^{(2)}_{3/2}(a_{\text{Sat}}/a)}{b^{(1)}_{3/2}(a_{\text{Sat}}/a)} e_{\text{Sat}}, \tag{11}$$

where $b^{(i)}_{3/2}$ are the Laplace coefficients. Plugging in the appropriate value, we find $e_{\text{forced}} = 0.14$. This should be an upper limit to the actual eccentricity of the ring because the collisions within the disk, which are not included in Eq. (11), should decrease eccentricity. We find the ring has an eccentricity of ~0.1, although the exact value changes over time. Thus, the ring seems to behaving reasonably. Interestingly, we also find that this ring's precession is negative, which implies that self-gravity is important to its dynamics. This, again, appears to be reasonable.

3.1.3. A system of growing embryos in the dispersion-dominated regime

As Goldreich et al. (2004a, 2004b) explained in detail, a system consisting of growing embryos in a sea of disk particles will be in one of two possible modes. If the velocity dispersion of the disk particles is large enough that the scale height of the planetesimal disk exceeds the radius of the embryo's Hill's sphere, $r_H = a(m_{\text{em}}/3\ M_\odot)^{1/3}$, then the disk behaves as if it is fully three-dimensional. This occurs if $u \gtrsim \Omega r_H$. This situation is referred to as the *dispersion-dominated* regime. However, if collisions damp planetesimal random velocities strongly enough, u can get much smaller than Ωr_H and the system enters the so-called *shear-dominated* regime. In this mode, growth proceeds in a qualitatively different way, and can be much more rapid than dispersion-dominated growth (also see Rafikov, 2004). In the extreme, the velocity dispersion can be so small that the entire vertical column of the planetesimal disk is within the protoplanet's Hill's sphere, thus making accretion a two-dimensional process.

Given the different nature of these two regimes, we test each of them separately. We begin with the dispersion-dominated regime. This test starts with a population of ten 5000 km radii embryos spread in semi-major axes between 25 and 35 AU. This implies that $\Sigma = 4.6 \times 10^{-4}\ M_\oplus/\text{AU}^2 = 0.012\ \text{g/cm}^2$. The initial eccentricities of the embryos were set to 0, but the inclinations were given a Raleigh distribution with an RMS $\sin(i)$ equal to 1.5×10^{-4} to insure that the embryo–embryo encounters can excite inclinations.

The disk was spread between 20 and 40 AU and was designed so that $\sigma = 1.5 \times 10^{-3}\ M_\oplus/\text{AU}^2$. We set $s = 100$ m. The disk was represented by at least 2000 tracers, where the eccentricities and inclinations were chosen from Raleigh distribution with an RMS eccentricity and $2\sin(i)$ equal to 0.025. Fig. 3 shows the temporal evolution of the eccentricities and inclinations of both the embryos (solid curves) and the disk particles (dotted curves) as observed in several runs where we varied N_{tracer} and N_{rings}.

Goldreich et al. (2004a, 2004b) predict that the eccentricities of both the embryos and disk particles would increase until a steady state is reached. This steady state is caused by a balance in the heating and cooling processes in both populations. The disk particles are being excited by the embryos, while they are being damped by collisions. At the same time, the embryos are exciting each other, while they are being damped due to dynamical friction with the disk particles. This steady state is clearly seen in our simulations (Fig. 3).

Indeed, Goldreich et al.'s (2004a, 2004b) analysis allows us to predict what the steady state eccentricities should be. In particular, in the regime of interest, Goldreich et al. (2004a, 2004b) find (Eq. (76)) that for the disk particles

$$u \sim v_{\text{esc}} \left(\frac{\Sigma}{\sigma}\frac{s}{R}\right)^{1/4}, \tag{12}$$

where v_{esc} is the escape velocity of the embryos. Plugging in the above values, we find that $u = 0.04\ \text{AU yr}^{-1}$, which corresponds to an RMS eccentricity of ~0.04 (the circular velocity at 30 AU is 1.1 AU yr^{-1} so that $e \sim u$). This is in excellent agreement with our simulation. For the embryos, if v is defined to be their velocity dispersion, then recently Chiang and Lithwick (2005, their Eq. (45)) showed that

$$\frac{v}{u} \sim \left(\frac{\Sigma}{8\sigma}\right)^{1/2}, \tag{13}$$

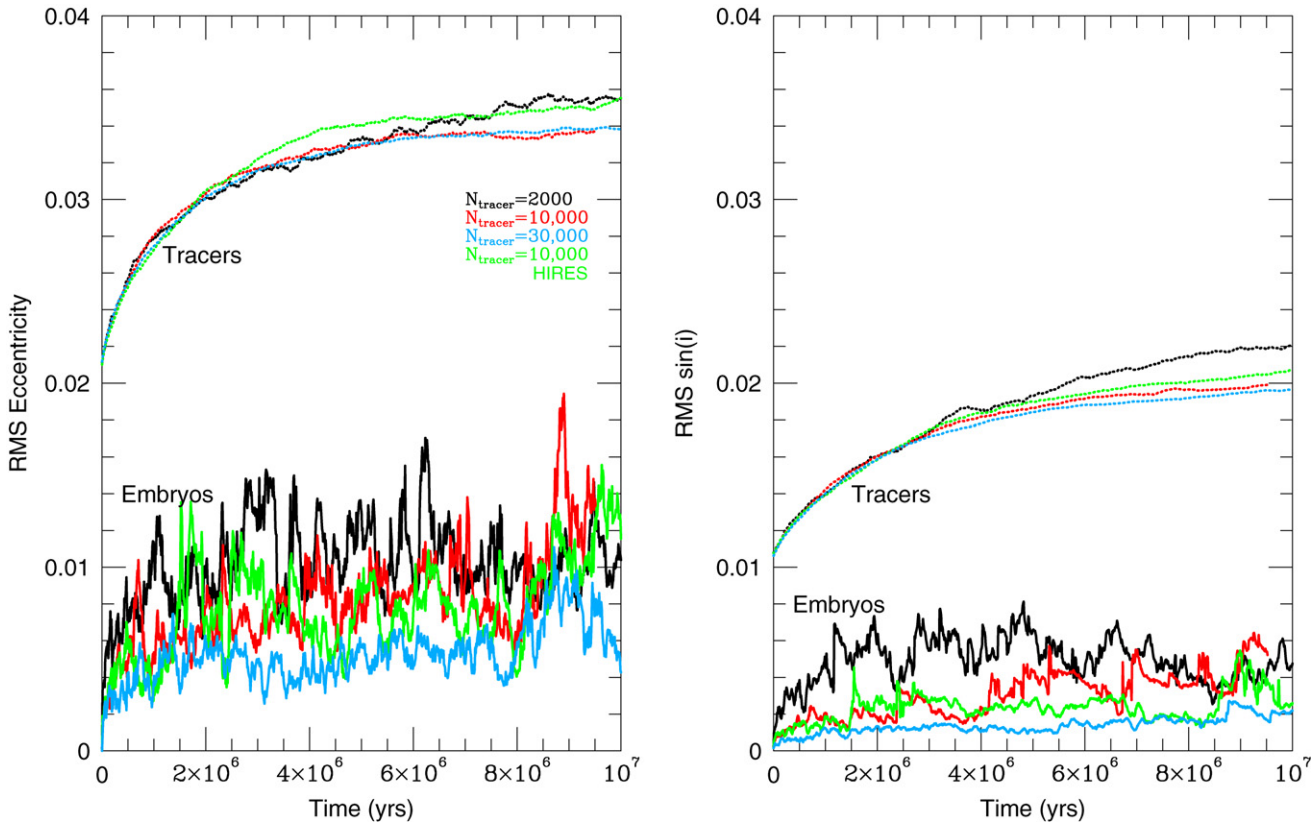

Fig. 3. The temporal evolution of the RMS eccentricity (left) and the RMS inclination (right) of a system of embryos embedded in a disk of small objects. The disk particles are collisionally active. The solid curves show the behavior of the embryos, while the dotted curves show that of the disk particles. Different colors refer to different disk resolutions, see text and legend for a description.

which is 0.2 in our test problem. We observe this ratio to be roughly 0.3. We believe that our simulations are reproducing the Goldreich et al.'s (2004a, 2004b) predictions fairly well given the order-of-magnitude nature of Goldreich et al.'s (2004a, 2004b) derivations.

As in our previous test, we must consider whether our code has high enough resolution. To investigate this issue, we performed four simulations where the only difference was the resolution of the disk. The black, red, and blue curves in Fig. 3 show the results for an increasing number of tracer particles (2000, 10,000, and 30,000, respectively). In all these cases $N_{\rm ring} = 1000$. In addition, the green curves (labeled 'HIRES') show the results for a simulation with 10,000 tracer particles, but where $N_{\rm ring} = 10{,}000$. In all cases the behavior of the systems are very similar. Indeed, the code has converged adequately enough, particularly when $N_{\rm tracers} \gtrsim 10{,}000$. As we discuss below, such resolutions are required in order to handle the shear-dominated regime.

We must also consider conserved quantities when testing our code. Unfortunately, collisions do not conserve energy, and so the only conserved quantity is the angular momentum vector of the system. In the run presented in Fig. 3, we find that angular momentum is conserved to 1 part in 10^4 over 100 Myr, which is satisfactory.

Finally, Goldreich et al. (2004a, 2004b) predict that the embryos will grow as they accrete the disk particles. In particular, their Eq. (77) predicts that

$$\frac{{\rm d}R}{{\rm d}t} \sim \frac{\Omega\sigma}{\rho_b}\left(\frac{\Sigma}{\sigma}\frac{s}{R}\right)^{-1/2}. \qquad (14)$$

For the parameters in this test, this predicts ${\rm d}R/{\rm d}t \sim 6 \times 10^{-6}$ km/yr. In the simulation, all embryos started with $R = 5000$ km. At the end of 10^7 years, Eq. (14) forecasts that the embryos should grow ∼50 km. We find at the end of the simulation that the average embryo radius is 5038 km. Again, the agreement is good.

3.1.4. A system of growing embryos in the shear-dominated regime

As a final test of our code, we study the behavior of a system containing three embryos with a mass of 0.17 $M_\oplus$ embedded in a 7 $M_\oplus$ disk of planetesimals spread from 27 to 33 AU. The radius of the disk particles was set to 5 cm. This problem was designed so that the system should be in the shear-dominated regime.

The results from several simulations with different disk resolutions is presented in Fig. 4. We start with a discussion of code convergence. We preformed simulations with $N_{\rm tracer}$ between 2000 and 32,700 particles. In almost all runs $N_{\rm rings} = 1000$, however we created one simulation with $N_{\rm rings} = 10{,}000$ (marked 'HIRES' in the figure). In all these calculations, we find that the behavior of the disk particles was the same. Thus,

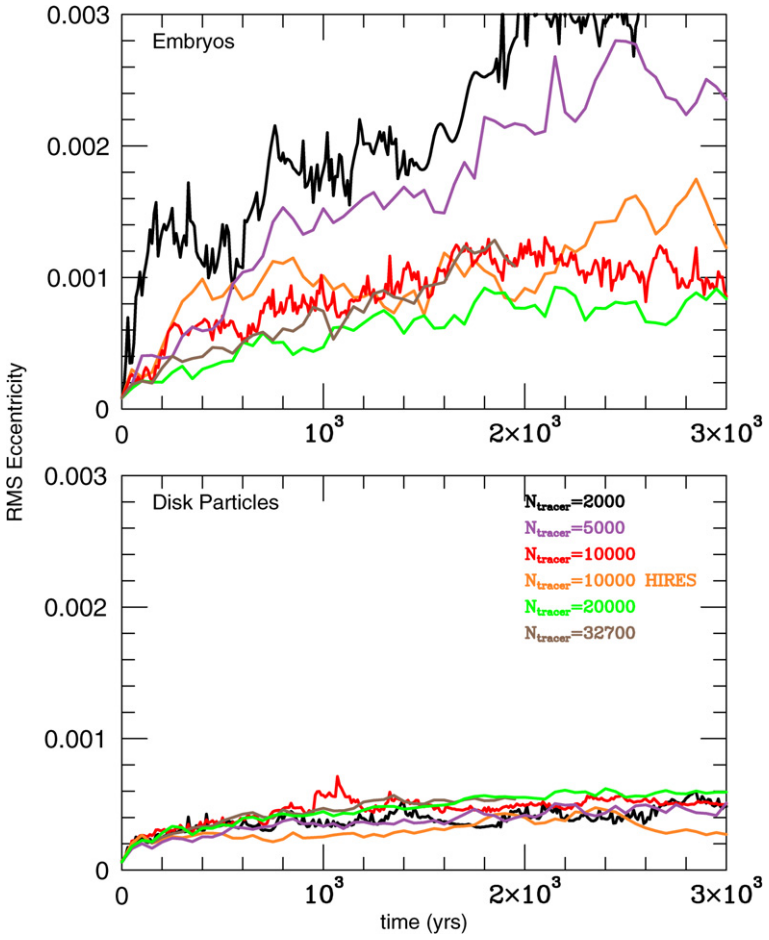

Fig. 4. The temporal evolution of the RMS eccentricity of a system of embryos embedded in a disk of small objects in the shear-dominated regime. The top panel shows the behavior of the embryos, while the bottom shows that of the disk particles. Different colors refer to different disk resolutions, see text and legend for a description.

we conclude that even in the highly damped shear-dominated regime, our collisional code has adequate resolution for all the cases we have studied.

The behavior of the embryos, on the other hand, only converged for $N_{\rm tracer} \gtrsim 10{,}000$. There are two reasons why the number of tracers can effect the dynamical state of the embryos. First, the code could be struggling to calculate accurately the dynamical friction of the tracers on the embryos. Equation (1) shows that the strength of dynamical friction should not depend on the size of the tracer particle if $m_{\rm em}/m_{\rm tr} \gg 1$, but the question is how big does this ratio have to be. Second, the embryos could be artificially excited due to the viscous stirring from the large tracers. In order for the code to behave correctly, the ratio of the tracer viscous stirring timescale to the viscous stirring timescale due to the embryos themselves must be greater than 1. Combining Goldreich et al.'s (2004a, 2004b) Eqs. (31) and (44), we expect that this ratio is proportional to $m_{\rm em}/m_{\rm tr}$, although again, it is not clear what this value needs to be in order to satisfy the timescale ratio constraint. The fact that the code converges for $N_{\rm tracer} \gtrsim 10{,}000$ implies that both the dynamical friction calculation is correct and the tracer viscous stirring is unimportant when $m_{\rm em}/m_{\rm tr} > 150$. We abide by this restriction in all the simulations that follow.

For the shear-dominated regime, Goldreich et al. (2004a, 2004b) predict (their Eq. (77))

$$u \sim \frac{v_{\rm esc}}{\alpha^{3/2}} \frac{\Sigma}{\sigma} \frac{s}{R}, \tag{15}$$

where α is the angular size of the Sun as seen from the embryo. In addition, Goldreich et al.'s (2004a, 2004b) Eq. (110) says

$$v \sim v_{\rm esc} \sqrt{\alpha} \frac{\Sigma}{\sigma}. \tag{16}$$

Plugging in the appropriate values for this test, we find that Goldreich et al. (2004a, 2004b) predict that $u \sim 2 \times 10^{-4}$ AU yr^{-1} and $v \sim 7 \times 10^{-4}$ AU yr^{-1}. In our simulation we find $u \sim 4 \times 10^{-4}$ AU yr^{-1} and, after convergence, $v \sim 10^{-3}$ AU yr^{-1}, which is in very good agreement with Goldreich et al.'s (2004a, 2004b) analytic theory.

In conclusion, in this subsection we presented a series of tests of SyMBA_COL. In all cases, the code reproduces the desired behavior. In addition, in those cases where direct comparison with Goldreich et al.'s (2004a, 2004b) derivations is appropriate, there is reasonable quantitative agreement, within a factor of a few. This level of agreement is about what one should expect given the order-of-magnitude nature of Goldreich et al.'s (2004a, 2004b) development. Thus, in the remainder

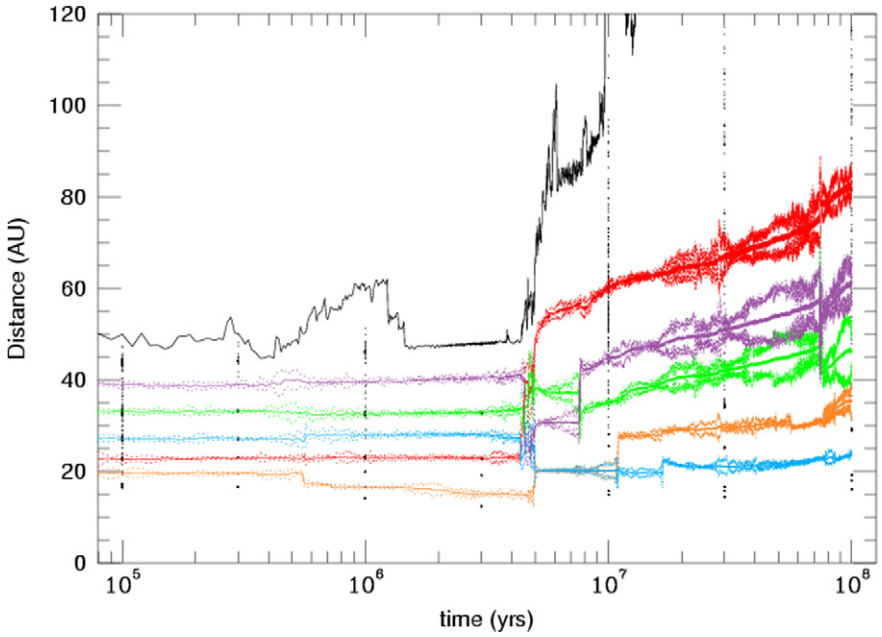

Fig. 5. $s = 1$ m and $m_d = 80\ M_\oplus$. The ice giants had an original mass of 16 $M_\oplus$. We plot three curves for each planet, which is represented by a different color. These curves show the semi-major axis, perihelion, and aphelion distances. The solid black curve illustrates the semi-major axis of the outermost disk particle. The columns of black points show the semi-major axes of all the disk particles at various times.

of the paper we employ the code to test Chiang et al.'s (2007) scenario for the early sculpting of the Kuiper belt.

4. Systems with five ice giants

In this section we use SyMBA_COL to perform full dynamical calculations of the scenario reviewed in Section 2. In particular, for reasons discussed in Section 2, we concentrate on the phase when the ice-giant system becomes unstable. Thus, we start our systems with a series of ice giants, each of which is 16 $M_\oplus$, spread from 20 to 35 AU, which corresponds to a spacing of roughly 5 Hills spheres. In all cases, the initial eccentricities and inclinations of the ice giants were very small ($\sim 10^{-4}$), and Jupiter and Saturn were included on their current orbits.

At the time of the instability, Chiang et al. (2007) predict that the mass of the planetesimal disk should be about the same as the total mass of the ice giants, i.e., 80 $M_\oplus$. However, given the nature of Goldreich et al.'s (2004a, 2004b) derivations, this number is very uncertain. Thus, we study a range of disk masses: $m_d = 40$, 80, 120, and 160 $M_\oplus$. In addition, it is uncertain what s should be, and thus we study two extremes: $s = 1$ m and 1 cm. The simulations initially contain 2000 tracer particles which are spread from 16 to 45 AU. The initial eccentricities of the disk particles were set to $\sim 10^{-4}$, while the inclinations set to half of this value. These parameters put our code in a regime where its validity and convergence have been demonstrated in the tests in Section 3.1.

Except where noted, we integrated the systems for 10^8 yr, with a timestep of 0.4 yr. As described in Levison and Duncan (2000), SyMBA and thus SyMBA_COL have difficulty handling close encounters with the Sun. Therefore, we remove from the simulation any object the reaches a heliocentric distance less than 2 AU. In all, we performed 10 simulations.

We start the discussion of our results with the $s = 1$ m runs. In particular, perhaps the best way to begin is with a detailed description of the behavior on one single simulation. For this purpose we chose the $m_d = 80\ M_\oplus$ run since it is closest to Goldreich et al.'s (2004a, 2004b) nominal $\Sigma \sim \sigma$ situation. Fig. 5 shows the temporal evolution of the nominal simulation. In the figure each ice giant is represented by three curves of the same color. The curves show its semi-major axis, perihelion, and aphelion distances. The black curve shows the semi-major axis of the outermost disk particle. In addition to the curves, there are columns of points. These points show the semi-major axes of all the disk particles at that particular time.

The system remains relatively quiescent for the first 500,000 yr. During this time, the disk particles rearrange themselves so that a large fraction of them are in the trojan points of the ice giants. This behavior can be seen in the two leftmost column of dots in the figure. In addition, two rings of particles form immediately interior to and exterior to the embryos. Originally the embryo growth rate is large, the embryo mass increases 1.1 $M_\oplus$, on average, in the first 60,000 yr. But after that time, very little growth happens. Again, this is due to the fact that most of the mass of the disk is found in the trojan points of the embryo and in isolated rings where they are protected from the embryos. At 550,000 yr the system becomes mildly unstable and undergoes a 'spreading event' that moves the inner ice-giant inward and the outer one outward. Such events are common in our simulations. After this event the eccentricities of the ice giants decrease presumably due to the fact that they are further from one another. For the next $\sim$4 myr the system is stable.

During this period of relative quiescence the disk particles concentrate in three main areas. Roughly 30% of the disk parti-

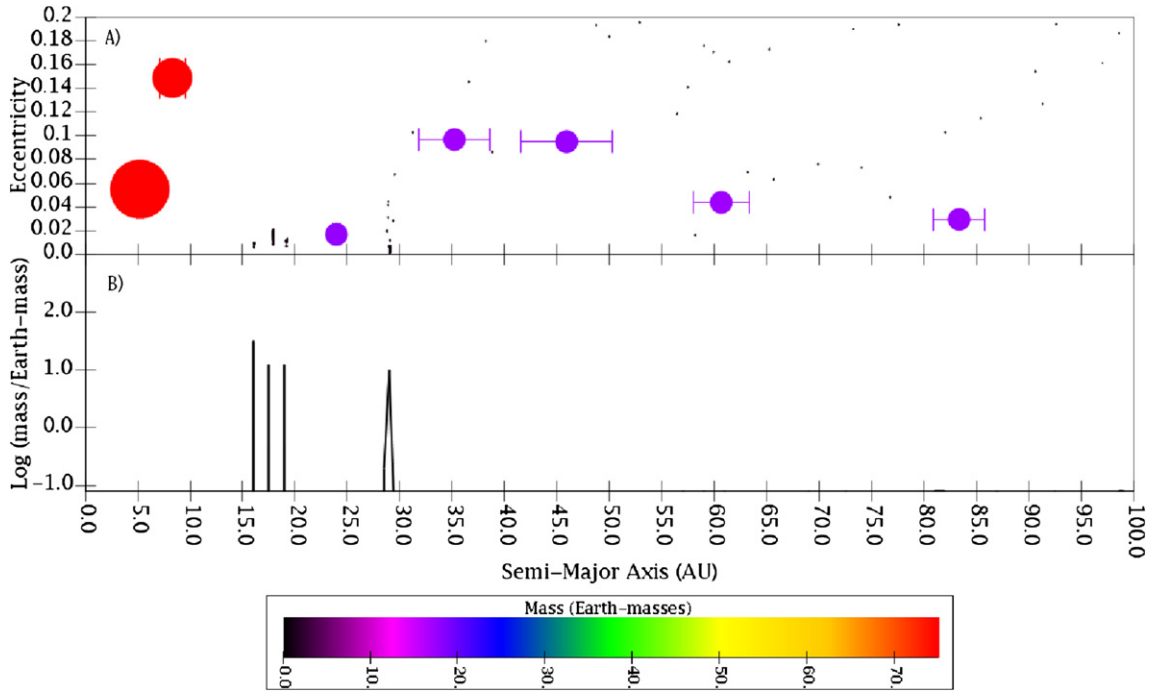

Fig. 6. The final state of five ice-giant simulations with $s = 1$ m and $m_d = 80\ M_\oplus$. (A) The eccentricity of an object as a function of its semi-major axes. The disk particles are shown as black dots. The planets are in color, the value of which is a function of the planet's mass. The legend for the color is shown below the plot. For the planets, the radius of the dot scales as the cube root of its mass. The 'error-bars' show the radial extent that the object travels as it orbits due to its eccentricity. (B) A histogram of the mass distribution of disk particles. The width of the semi-major axis bins is 0.5 AU. Notice that almost all of the mass is concentrated in a few narrow rings.

cles can be found in a ring between the orange and red embryos. This ring therefore contains 22 $M_\oplus$! It is very narrow as well—only 0.05 AU in width. Roughly the same amount of material can be found in a ring at 47 AU, beyond all of the embryos. This ring is also very narrow with a width of only ∼0.1 AU. Finally, 29% of the disk can be found in the trojan points of the green embryo. This implies that there is more mass in the Lagrange points than in the embryo, itself. The characteristics of these structures leaves us wondering how physically realistic they are. After all, our code ignores fragmentation, which may be important as the ring forms. In addition, once the ring forms, the relative velocities are very small and the surface densities are large, thus we might expect either two-body accretion or a gravitational instability to form larger objects. We believe that the ring is an artifact of the simplistic collisional physics that we inherited from Goldreich et al. (2004a, 2004b) and they are probably not physical.

At 4.3 Myr, the red and green embryos in the figure hit the 4:3 mean motion resonance with one another. This destabilizes the embryos and they undergo a series of scattering events with one another. A large number of disk particles are released from their storage locations at this time. This period of violence lasts for 700,000 yr, but eventually the dynamical friction caused by the released disk particles is able to decouple the embryos from one another. Amusingly, the blue and orange embryos get trapped in the 1:1 mean motion resonance with one another, which lasts for over 5 myr.

During the remainder of the simulation, the ice giants migrate outward. The disk particles that were liberated during the instability are spread out enough that their collisional damping time is longer than the time between encounters with the embryos. Thus, the planets hand the particles off to one another allowing a redistribution of angular momentum. This process, which is called *planetesimal-driven migration* is well understood (see Levison et al., 2006 for a review) since it was discovered over 20 yr ago (Fernández and Ip, 1984) and has been studied as a possible explanation of the resonant structure of the Kuiper belt (Malhotra, 1995; Hahn and Malhotra, 2005).

However, collisional damping still does play a role during this time. As the planets migrate, four relatively high mass rings start to form. At the end of the simulation the most massive of these contain 32 $M_\oplus$! Indeed, the final system is shown in Fig. 6. Fig. 6A shows the eccentricity of objects as a function of their semi-major axis. The planets are in color, with the 'error-bars' showing the range of heliocentric distances that they travel as they orbit. We find that the inclinations, which are not shown, are roughly what one would expect—i.e., the $\sin(i)$'s are roughly half the eccentricities. This is a general result that we see in all the runs.

The size of the symbol in the figure scales as the mass of the planet to the 1/3 power. The disk particles are shown in black. Fig. 6B presents a histogram of the mass of the disk particles as a function of semi-major axis. There are three important things to note about the final system: (1) None of the ice giants were ejected from the system. (2) There is a planet in a nearly circular orbit at a large heliocentric distance (although it is close enough that if it actually existed it would have been discovered long ago). Although this system may not be finished evolving, it is very unlikely that this planet will be removed. (3) Almost all the disk particles survive. Of the 80 $M_\oplus$ of material in the disk,

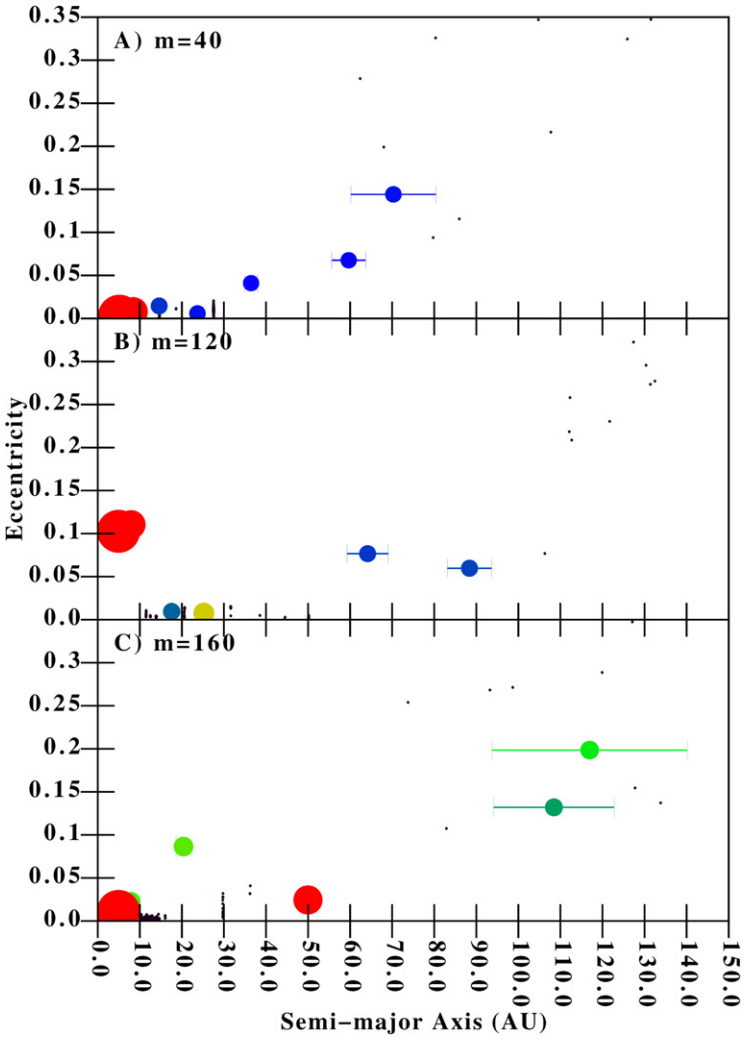

Fig. 7. The final state of five ice-giant simulations with $s = 1$ m not shown in Fig. 6. See Fig. 6A for a description of this type of plot. (A) 40 $M_\oplus$ disk. (B) 120 $M_\oplus$ disk. (C) 160 $M_\oplus$ disk.

72 $M_\oplus$ are still present at 100 Myr. Almost all of this mass is found in four massive rings interior to 30 AU.

We performed 3 other simulations with $s = 1$ m and the stories for these simulations are, for the most part, very similar. The final states of these systems are shown in Fig. 7. This figure is the same as Fig. 6A, which fits in the sequences between Figs. 7A and 7B. The first thing to note is that the entire planetary system went unstable in the $m_d = 160$ $M_\oplus$ run. In this case, a 75 $M_\oplus$ ring formed in Saturn's 1:2 mean motion resonance that eventually drove up Saturn's eccentricity until the Jupiter–Saturn system was disrupted. We will ignore this run in the following analysis because it clearly cannot represent what happened in the Solar System. There were no planetary ejections in any of these simulations in the remaining runs. There was one merger in the $m_d = 120$ $M_\oplus$ run. In all cases, we find massive planets at large heliocentric distances, inconsistent with the current Solar System and the expectations of Goldreich et al. (2004a, 2004b) and Chiang et al. (2007).

As we described above, we are interested in setting up our initial conditions so that they represent Chiang et al.'s (2007) hypothetical Solar System immediately before the instability sets in, when the ice giants are presumably almost fully formed. That is reason we started with systems where the initial mass of the ice giants was set to 16 $M_\oplus$. Thus, to test this assumption it is interesting to look at the amount of mass accreted by the ice giants during our calculations. The colors in Figs. 6A and 7 indicate the mass of the planet. We found that between 10 and 16% of the original disk mass is accreted by the ice giants in our $s = 1$ m runs. The amount of embryo growth increases monotonically with disk mass. The ice giants in the $m_d = 40$ $M_\oplus$ run only accreted a total of 6.5 $M_\oplus$ of planetesimals, while they grew roughly by a total of 13 $M_\oplus$ in the $m_d = 120$ $M_\oplus$ simulation run. The planets in this run are probably too large to be considered good Uranus and Neptune analogs. It is also interesting to note that the more massive the disk, the more excited the final system of ice giants is. We think that this is due to the fact that the more massive disks produce larger planets, which, in turn, produce stronger mutual perturbations, and thus stability is achieved only with wider orbital separations.

We now turn our attention to the $s = 1$ cm runs—the results of which are shown in Fig. 8. The same basic dynamics that

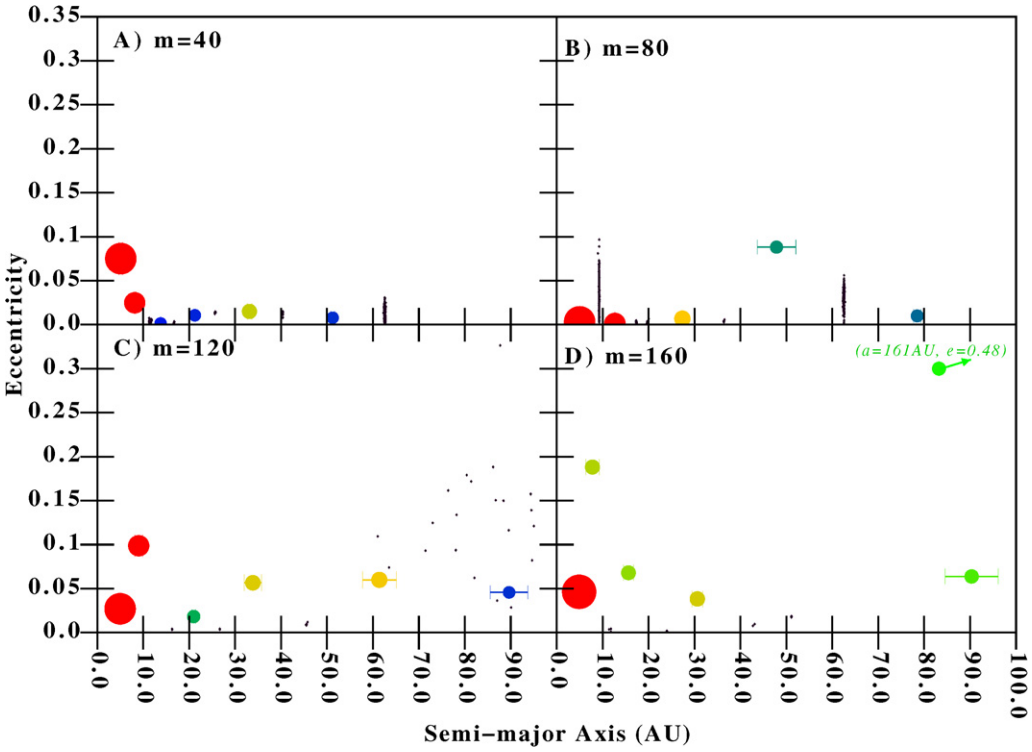

Fig. 8. The final state of five ice-giant simulations with $s = 1$ cm. These are the runs where the initial mass of the planets was 16 $M_\oplus$. See Fig. 6A for a description of this type of plot. (A) 40 $M_\oplus$ disk. (B) 80 $M_\oplus$ disk. (C) 120 $M_\oplus$ disk. (D) 160 $M_\oplus$ disk. The ice giant in the upper right of this panel should actually be at $a = 161$ AU and $e = 0.48$. It is plotted at its perihelion distance rather than semi-major axis.

we discussed above work with these systems and we get the same basic results. This includes the fact that Jupiter and Saturn went unstable in the $m_d = 160$ $M_\oplus$ run. The main difference between the $m_d \leqslant 120$ $M_\oplus$ runs here and those in the $s = 1$ m is that in these runs the ice giants accreted much more of the disk material. For example, the ice giants in the $m_d = 120$ $M_\oplus$ run accreted a total of 37 $M_\oplus$ of planetesimals in the $s = 1$ cm run, while they accreted 13 $M_\oplus$ in the $s = 1$ m simulation. This is probably due to the fact that, at least at early times, collisions between the disk particles are more frequent and thus the system remains cooler. As a result, the gravitational focusing factor of the ice giants remains larger so that the accretion rate is higher. As a consequence, the final ice-giant systems that we obtain in these runs are, for the same initial disk mass, more excited and spread out than those constructed in the $s = 1$ m simulations (Fig. 7).

In response to the large accretion rates in our $s = 1$ cm runs, we decided to push our simulation back to an earlier time in order to determine if we can produce ice giants on the order of the same size as Uranus and Neptune for this value of s. In particular, our systems started with five embryos of 8.3 $M_\oplus$ each. The orbits of the embryos and the geometry of the disk was the same as in our previous integrations. We preformed 4 simulations with $m_d = 43$, 85, 128, and 170 $M_\oplus$. As with the previous cases, the orbits of Jupiter and Saturn became unstable in the high disk mass. Not surprisingly, we found a monotonic relationship between the initial disk mass and the amount of material the ice giants accreted from the disk in the remaining systems. In particular, on average each ice giant accreted 2, 6, and 16 $M_\oplus$ in the runs with $m_d = 43$, 85, and 128 $M_\oplus$, respectively. Since we started with embryos of 8.3 $M_\oplus$, the $m_d = 85$ $M_\oplus$ disk produces the best planets. However, we believe that larger disk masses would still probably acceptable if we were to increased s (thereby decreasing the damping). On the other hand, since $s = 1$ cm is so extreme, we believe that we can rule out less massive disks (i.e., $m_d \lesssim 50$ $M_\oplus$)—these anemic disks are unlikely to form objects as massive as Uranus and Neptune.

The final systems are shown in Fig. 9. As the planets grew, their orbits spread. The final systems always had a planet well beyond 30 AU.

5. System with Earth-mass embryos

Finally, in this section we briefly study the growth of the ice giants from much smaller planetary embryos. Our goal here is to make sure that the initial conditions used above were not artificial in some respect. That is, given the order-of-magnitude nature of Goldreich et al.'s (2004a, 2004b) arguments, perhaps we start the above calculations in the wrong state. For example, in all the above runs, we started with five ice giants, as suggested by Chiang et al. (2007). However, perhaps the natural system should contain four such objects, rather than five, and then the system might evolve as Chiang et al. (2007) suggested. Thus, in this section we present simulations where we start with small planetary embryos and let the system evolve naturally. Unfortunately, these simulations are computationally expensive and thus we can only perform a couple of test cases.

In particular, our systems started with 6 embryos of 1 $M_\oplus$ each, spread from 21 to 27 AU. The initial eccentricities and in-

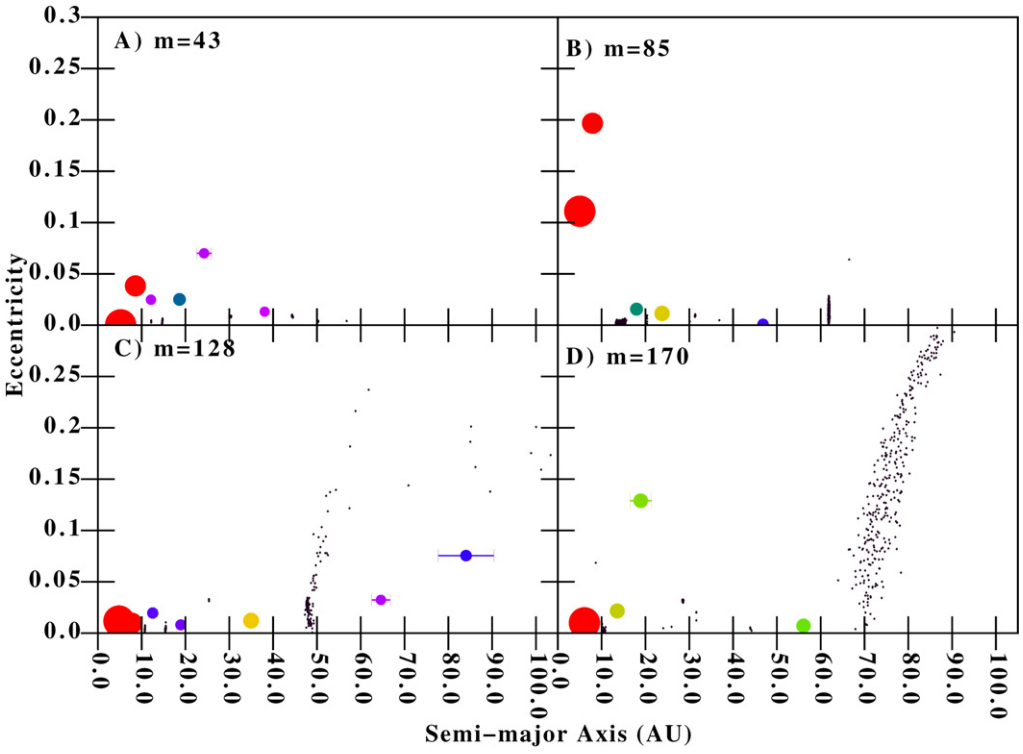

Fig. 9. The final state of five ice-giant simulations with $s = 1$ cm. These are the runs where the initial mass of the ice giants was 8.3 $M_\oplus$. See Fig. 6A for a description of this type of plot. (A) 43 $M_\oplus$ disk. (B) 85 $M_\oplus$ disk. (C) 128 $M_\oplus$ disk. (D) 170 $M_\oplus$ disk.

clinations of these particles are very small ($\sim 10^{-3}$). These objects were embedded in a disk of 18,000 tracer particles spread from 20 to 30 AU, with a total mass of 90 $M_\oplus$. Two simulations were done, one with $s = 1$ m and one with $s = 1$ cm.

Performing a computation with 18,000 tracer particles is very CPU intensive. We needed such a large number of tracers to adequately resolve the dynamical friction between the tracers and embryos, which, as we explained above, requires that $m_{\rm em}/m_{\rm tr} > 150$. However, as the embryos grow, such a large number of tracers were no longer needed. Thus, our plan was to continue the integrations until the average embryo mass was 10 $M_\oplus$, after which we would remove four out of every five tracer particles at random while keeping the total mass of tracers constant.

Fig. 10 shows the temporal evolution of the average embryo mass in both the simulations. The dotted curve is from the $s = 1$ m. Note that the growth rate is very small—the average mass of the embryos at 2.5 Myr was only 1.2 $M_\oplus$. In addition, during the last 500,000 years of the simulation, the growth rate was only 3×10^{-9} $M_\oplus\,{\rm yr}^{-1}$. We terminated the simulation at this point because it was clear that this simulation was no going to produce Uranus- and Neptune-sized planets fast enough. This is true because Uranus and Neptune, their ice-giant status notwithstanding, do each have several $M_\oplus$ of H and He in their atmospheres. The most natural way to account for this is if these planets finished their accretion in $\sim 10^7$ yr, before the gas nebula was completely depleted (Haisch et al., 2001).

As Fig. 10 shows, however, the $s = 1$ cm runs, indeed, produce reasonable Uranus and Neptune analogs within 10 Myr.

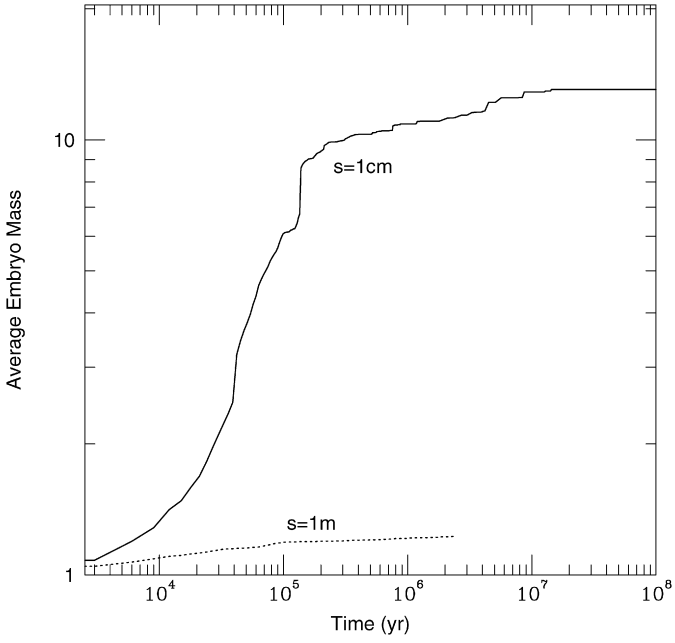

Fig. 10. The average mass of the embryos as a function of time in our simulations which starts with six 1-Earth-mass embryos. The solid and dotted curves refer to the $s = 1$ cm and $s = 1$ m, respectively. The $s = 1$ m run was terminated at 2.5 Myr because of very small growth rates.

In fact, by this time, the embryos have an average mass of 12.4 $M_\oplus$. The final system is shown in Fig. 11. At 100 Myr, this run has four ice giants ranging in mass from 10.6 to 14.9 $M_\oplus$. Recall that the system started with six embryos. There were two mergers that reduced the number to four. Thus, none of the

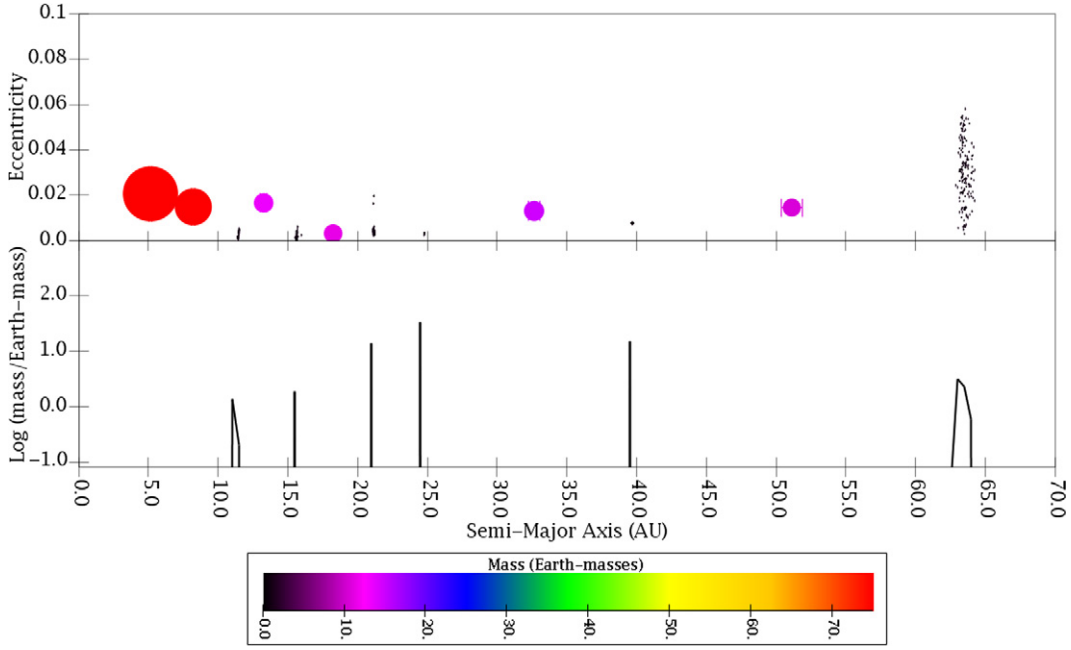

Fig. 11. The final state of our $s = 1$ cm simulation with Earth-mass embryos. See Fig. 6 for a description of this type of plot.

ice giants were ejected. Two of the resulting planets have semi-major axes beyond the current orbit of Neptune. Of particular note is the 10.6 $M_\oplus$ ice giant on an orbit with a semi-major axis of 51 AU and an eccentricity of 0.01. This system suffers from another problem as well. Less than 50% of the tracers were accreted by the planets. Thus, there is still 46 $M_\oplus$ of material concentrated in narrow rings throughout the outer planetary system.

6. Conclusions

Chiang et al. (2007) have recently proposed a new and innovative scenario for the primordial sculpting of the Kuiper belt. The idea is based on a recent pair of papers, Goldreich et al. (2004a) and Goldreich et al. (2004b), that, based on order-of-magnitude analytic arguments, predicted that originally ∼5 planets began to grow between ∼20 and ∼40 AU. As these planets grew to masses of ∼15 $M_\oplus$ their orbits went unstable, some of them were ejected, leaving Uranus and Neptune in their current orbits. Chiang et al. (2007) argued that this violent process could explain the the currently observed dynamical excitation of the Kuiper belt. Like Goldreich et al. (2004a, 2004b), the Chiang et al.'s (2007) scenario was not tested with numerical simulations, but was solely supported by back-of-the-envelope analytic estimates.

Therefore, here we presented a series of integrations intended to simulate numerically Chiang et al.'s (2007) scenario. We performed 12 simulations starting at the stage where the 5 ice giants are predicted to become unstable. In these simulations we varied the mass contained in the background disk, the size of the disk particles (either 1 m or 1 cm), and the initial mass of the ice giants. We found that in the simulations in which the mass of the disk $\gtrsim$160 $M_\oplus$, the orbits of Jupiter and Saturn were not stable. In addition, we can rule out systems with disk masses $\lesssim$50 $M_\oplus$ because our simulations that start with 8.3 $M_\oplus$ ice giants show that these disks are unlikely to produce planets as large as Uranus and Neptune.

In the runs where Jupiter and Saturn were stable, contrary to Goldreich et al.'s (2004a, 2004b) conjecture, planetary ejection almost never occurs. Instead, we found that the planetary systems spread and thus all our final systems contained a planet in an orbit far beyond the current orbit of Neptune (but still at a distance at which it would not escape detection). All our systems had at least one planet beyond 50 AU. Indeed, the semi-major axis of the outermost giant planet in these systems ranged from 52 to 90 AU.

Obviously, we have not been able to model all possible cases since parameter space is large and these calculations are expensive. However, we think that it is possible to speculate how these results would change if we expanded our coverage of parameter space. It would help if we were to reduce the number of ice giants to four, or even three, because we would need to eject fewer planets. However, since we found only one ejection in our entire set of simulations (only including those runs where Jupiter and Saturn were stable), we do not believe that this would solve the problem.

It might also help if we were to make the initial planetary system more compact and thus make it more likely that the ice giants would evolve onto Saturn-crossing orbits. However, we find that for the disk masses we have studied, Saturn only has a 17% chance of ejecting an ice giant that is crossing its orbit. Therefore, a more compact system probably will not solve the problem. This conclusion is at odds with the results of Thommes et al. (1999, 2002), where ice giants originally in compact planetary systems were commonly ejected. We believe that this difference is due to the fact that our disks are collisionally active. In the Thommes et al. simulations, disk particles are very quickly removed as the result of gravitational interaction

with the planets. This does not occur in our simulations because collisions keep the disk in place. This discussion leads, however, to the final way in which we could increase the number of ejections—we could increase s thereby making these simulations more like those in Thommes et al. (1999, 2002). However, we find that even in our $s = 1$ m runs, the accretion rate is so small that in a situation where s is large, Uranus and Neptune would probably not grow (see Levison and Stewart, 2001), at least by Goldreich et al.'s (2004a, 2004b) mechanism.

As a case in point, we performed two simulations that initially contained six 1-Earth-mass embryos embedded in a 90 $M_\oplus$ disk. One run had $s = 1$ m, and the other had $s = 1$ cm. In the $s = 1$ m run, the growth rates were too small to allow Uranus–Neptune analogs to form in a reasonable amount of time. However, four ice giants with masses between 10.6 and 14.9 $M_\oplus$ formed in the $s = 1$ cm run. The outermost of these had a semi-major axis of 51 AU and an eccentricity of 0.01.

All the simulations we have performed show the same basic behavior—the system spreads during the growth and dynamical evolution of the ice giants. Planetary ejections are rare. For reasons described above, we believe these results are generic enough to be universal. Therefore, we believe that it is safe to rule out the Chiang et al.'s (2007) scenario for the sculpting of the Kuiper belt, as well as Goldreich et al.'s (2004a, 2004b) scenario for the formation of Uranus and Neptune.

We think that the problem with Goldreich et al. (2004a, 2004b) is not in the derivation of the various estimates, but rather in some of simplifying assumptions that they were forced to employ to make the problem analytically tractable. Indeed, on microscopic, short-term, scales, we were able to reproduce much of the behavior that Goldreich et al. (2004a, 2004b) predicted (see Section 3). In the case of the problem we address in this paper, Goldreich et al.'s (2004a, 2004b) assumption that the surface density of the disk particles remains smooth and uniform is probably at fault, since we find that the formation of rings and gaps actually dominates the dynamics. Having said this, we must remind the reader that we adopted many of Goldreich et al.'s (2004a, 2004b) simplifying assumption ourselves, and if this mechanism for planet formation is to be further explored, these should be more fully tested.

Acknowledgments

H.F.L. is grateful for funding from NASA's Origins and PGG programs. A.M. acknowledges funding from the French National Programme of Planetology (PNP). We also thank John Chambers, Eiichiro Kokubo, and an anonymous third person for acting as referees on this manuscript. Their comments were much appreciated. Finally, we thank Glen Stewart and Bill Ward for useful discussions.

References

Allen, R.L., Bernstein, G.M., Malhotra, R., 2001. The edge of the Solar System. Astrophys. J. 549, L241–L244.

Allen, R.L., Bernstein, G.M., Malhotra, R., 2002. Observational limits on a distant cold Kuiper belt. Astron. J. 124, 2949–2954.

Bernstein, G.M., Trilling, D.E., Allen, R.L., Brown, M.E., Holman, M., Malhotra, R., 2004. The size distribution of trans-neptunian bodies. Astron. J. 128, 1364–1390.

Binney, J., Tremaine, S., 1987. Galactic Dynamics. Princeton Univ. Press, Princeton, NJ.

Brouwer, D., Clemence, G.M., 1961. Methods of Celestial Mechanics. Academic Press, New York.

Brown, M.E., 2001. The inclination distribution of the Kuiper belt. Astron. J. 121, 2804–2814.

Chambers, J., 2006. A semi-analytic model for oligarchic growth. Icarus 180, 496–513.

Chandrasekhar, S., 1943. Dynamical friction. I. General considerations: The coefficient of dynamical friction. Astrophys. J. 97, 255–262.

Chiang, E.I., Brown, M.E., 1999. Keck pencil-beam survey for faint Kuiper belt objects. Astron. J. 118, 1411–1422.

Chiang, E.I., Lithwick, Y., 2005. Neptune Trojans as a test bed for planet formation. Astrophys. J. 628, 520–532.

Chiang, E., Lithwick, Y., Murray-Clay, R., Buie, M., Grundy, W., Holman, M., 2007. A brief history of trans-neptunian space. In: Protostars and Planets V, pp. 895–911.

Duncan, M.J., Levison, H.F., Lee, M.H., 1998. A multiple time step symplectic algorithm for integrating close encounters. Astron. J. 116, 2067–2077.

Fernández, J.A., Ip, W.-H., 1984. Some dynamical aspects of the accretion of Uranus and Neptune—The exchange of orbital angular momentum with planetesimals. Icarus 58, 109–120.

Gladman, B., Kavelaars, J.J., Petit, J.-M., Morbidelli, A., Holman, M.J., Loredo, T., 2001. The structure of the Kuiper belt: Size distribution and radial extent. Astron. J. 122, 1051–1066.

Goldreich, P., Lithwick, Y., Sari, R., 2004a. Final stages of planet formation. Astrophys. J. 614, 497–507.

Goldreich, P., Lithwick, Y., Sari, R., 2004b. Planet formation by coagulation: A focus on Uranus and Neptune. Annu. Rev. Astron. Astrophys. 42, 549–601.

Gomes, R.S., 2003. The origin of the Kuiper belt high-inclination population. Icarus 161, 404–418.

Gomes, R., Levison, H.F., Tsiganis, K., Morbidelli, A., 2005. Origin of the cataclysmic Late Heavy Bombardment period of the terrestrial planets. Nature 435, 466–469.

Hahn, J.M., Malhotra, R., 1999. Orbital evolution of planets embedded in a planetesimal disk. Astron. J. 117, 3041–3053.

Hahn, J.M., Malhotra, R., 2005. Neptune's migration into a stirred-up Kuiper belt: A detailed comparison of simulations to observations. Astron. J. 130, 2392–2414.

Haisch Jr., K.E., Lada, E.A., Lada, C.J., 2001. Disk frequencies and lifetimes in young clusters. Astrophys. J. 553, L153–L156.

Jewitt, D., Luu, J., Chen, J., 1996. The Mauna Kea–Cerro–Tololo (MKCT) Kuiper belt and centaur survey. Astron. J. 112, 1225–1238.

Kenyon, S.J., Luu, J.X., 1998. Accretion in the early Kuiper belt. I. Coagulation and velocity evolution. Astron. J. 115, 2136–2160.

Kenyon, S.J., Luu, J.X., 1999. Accretion in the early outer Solar System. Astrophys. J. 526, 465–470.

Kokubo, E., Ida, S., 1996. On runaway growth of planetesimals. Icarus 123, 180–191.

Kokubo, E., Ida, S., 1998. Oligarchic growth of protoplanets. Icarus 131, 171–178.

Levison, H.F., Duncan, M.J., 2000. Symplectically integrating close encounters with the Sun. Astron. J. 120, 2117–2123.

Levison, H.F., Morbidelli, A., 2003. The formation of the Kuiper belt by the outward transport of bodies during Neptune's migration. Nature 426, 419–421.

Levison, H.F., Stern, S.A., 2001. On the size dependence of the inclination distribution of the main Kuiper belt. Astron. J. 121, 1730–1735.

Levison, H.F., Stewart, G.R., 2001. Remarks on modeling the formation of Uranus and Neptune. Icarus 153, 224–228.

Levison, H.F., Lissauer, J.J., Duncan, M.J., 1998. Modeling the diversity of outer planetary systems. Astron. J. 116, 1998–2014.

Levison, H.F., Morbidelli, A., Gomes, R., Backman, D., 2006. Planet migration in planetesimal disks. In: Protostars and Planets V, pp. 669–684.

Malhotra, R., 1995. The origin of Pluto's orbit: Implications for the Solar System beyond Neptune. Astron. J. 110, 420–429.

Miller, R.H., 1978. Numerical experiments on the stability of disklike galaxies. Astrophys. J. 223, 811–823.

Morbidelli, A., 2005. Origin and dynamical evolution of comets and their reservoirs. ArXiv Astrophys. e-print arXiv:astro-ph/0512256.

Morbidelli, A., Jacob, C., Petit, J.-M., 2002. Planetary embryos never formed in the Kuiper belt. Icarus 157, 241–248.

Morbidelli, A., Brown, M.E., Levison, H.F., 2003. The Kuiper belt and its primordial sculpting. Earth Moon Planets 92, 1–27.

Murray, C.D., Dermott, S.F., 2000. Solar System Dynamics. ISBN 0521575974.

Ohtsuki, K., Ida, S., 1990. Runaway planetary growth with collision rate in the solar gravitational field. Icarus 85, 499–511.

Rafikov, R.R., 2004. Fast accretion of small planetesimals by protoplanetary cores. Astron. J. 128, 1348–1363.

Skeel, R.D., Biesiadecki, J.J., 1994. Symplectic integration with variable stepsize. Ann. Numer. Math. 1, 191–199.

Stern, S.A., 1996. On the collisional environment, accretion time scales, and architecture of the massive, primordial Kuiper belt. Astron. J. 112, 1203–1224.

Stern, S.A., Colwell, J.E., 1997. Accretion in the Edgeworth–Kuiper belt: Forming 100–1000 km radius bodies at 30 AU and beyond. Astron. J. 114, 841–849.

Tegler, S.C., Romanishin, W., 2003. Resolution of the Kuiper belt object color controversy: Two distinct color populations. Icarus 161, 181–191.

Thommes, E.W., Duncan, M.J., Levison, H.F., 1999. The formation of Uranus and Neptune in the Jupiter–Saturn region of the Solar System. Nature 402, 635–638.

Thommes, E.W., Duncan, M.J., Levison, H.F., 2002. The formation of Uranus and Neptune among Jupiter and Saturn. Astron. J. 123, 2862–2883.

Thommes, E.W., Duncan, M.J., Levison, H.F., 2003. Oligarchic growth of giant planets. Icarus 161, 431–455.

Trujillo, C.A., Brown, M.E., 2001. The radial distribution of the Kuiper belt. Astrophys. J. 554, L95–L98.

Trujillo, C.A., Brown, M.E., 2002. A correlation between inclination and color in the classical Kuiper belt. Astrophys. J. 566, L125–L128.

Trujillo, C.A., Jewitt, D.C., Luu, J.X., 2001. Properties of the trans-neptunian belt: Statistics from the Canada–France–Hawaii Telescope survey. Astron. J. 122, 457–473.

Tsiganis, K., Gomes, R., Morbidelli, A., Levison, H.F., 2005. Origin of the orbital architecture of the giant planets of the Solar System. Nature 435, 459–461.

Wisdom, J., Holman, M., 1991. Symplectic maps for the n-body problem. Astron. J. 102, 1528–1538.

Youdin, A.N., Chiang, E.I., 2004. Particle pileups and planetesimal formation. Astrophys. J. 601, 1109–1119.

Youdin, A.N., Shu, F.H., 2002. Planetesimal formation by gravitational instability. Astrophys. J. 580, 494–505.